Int J Cardiovasc Imaging (2018) 34:3–14
DOI 10.1007/s10554-017-1235-7

ORIGINAL PAPER

Myocardial T1 mapping and extracellular volume quantification: an overview of technical and biological confounders

Stefan K. Piechnik[1] · **Michael Jerosch-Herold**[2]

Received: 7 August 2017 / Accepted: 10 August 2017 / Published online: 28 August 2017

Abstract Novel tissue biomarkers based on the spin–lattice relaxation time T1, a fundamental property in the theory of magnetic resonance physics, have emerged as a new approach for myocardial tissue characterization with many validated clinical applications. This article is intended as an overview of the physical and physiological mechanisms underlying the interpretation and the accuracy of any practical measurement of T1, or derived biomarkers such as extravascular volume fraction, and also includes a discussion of potential pitfalls. Numerous caveats und knowledge gaps related to the precise interpretation of T1-based biomarkers remain, which are being addressed incrementally through ongoing research. Equally important, further careful standardization will pave the way for a wider clinical translation of these novel T1-based biomarkers of tissue remodeling, which have been well validated for their sensitivity to pathophysiological changes, though for the most part in single-center studies.

Keywords T1 · Myocardium · Relaxation · Fibrosis · Extracellular matrix

✉ Michael Jerosch-Herold
mjerosch-herold@bwh.harvard.edu

[1] Oxford Centre for Clinical Magnetic Resonance Research, Division of Cardiovascular Medicine, Radcliffe Department of Medicine, University of Oxford, John Radcliffe Hospital, Oxford OX39DU, UK

[2] Brigham and Women's Hospital, and Harvard Medical School, 15 Francis Street, Boston, MA 02115, USA

Introduction

The T1 spin–lattice relaxation time is a fundamental property in magnetic resonance physics. In simple systems, like aqueous ionic solutions, a single T1 time constant accurately describes the relaxation of the longitudinal magnetization component. Despite many caveats, the general idea has proven extremely useful when applied to complex systems, including living tissue. In particular the applications of spatially resolved T1 mapping have over the last decade evolved into a powerful approach for myocardial tissue characterization [1]. The biomarkers derived from T1 mapping have been widely validated in clinical studies for indications where myocardial tissue remodeling represents an important aspect of the underlying pathology. This rapid rise to prominence in the field of cardiac magnetic resonance (CMR) would not have been possible without a slew of technical developments that addressed the challenges in measuring and displaying T1 in the heart. That these technical enhancements were of critical importance can be judged by the fact that T1 effects of ischemia, edema and loss of viability in myocardial tissue were recognized since the inception of cardiac MRI [2–4]. T1 measurements have been used for stationary organs like the brain, yet cardiac T1 mapping only took off after some key technical advances had been made. CMR users now have various techniques for T1 imaging/mapping at their disposal, though these techniques do not necessarily provide T1 values in close agreement. In fact, the quest for technical advances has led to the realization that there is a close interaction between T1 as tissue property, and the technique that is used for its measurement. It therefore stands to reason that proper tissue characterization by T1 mapping requires an understanding of the techniques being employed. The goal of this article is to provide an

overview of the evolution of T1 mapping technology, concentrating in particular on the pitfalls of the most commonly used clinical techniques and their use as markers of particular pathophysiological changes.

Theoretical basis for T1 estimation

T1 measurements refer to the process of determining the characteristic time for magnetization recovery after application of a radio-frequency (RF) pulse that changes the spin magnetization from its equilibrium state. In its purest form, both magnetization preparation and read-out of a signal are repeated for a series of time points after the magnetization preparation, with proper time left between repetitions to ensure that before each magnetization preparation the spins have returned to their equilibrium state. In practice, an inversion pulse (180°) or a saturation pulse (90°) are most frequently used to change the magnetization away from its equilibrium state. The evolution of the longitudinal magnetization component (M_z) after changing the magnetization from its equilibrium state is described by an exponential function of time:

$$M_z(t) = A - B \cdot \exp\left(-\frac{t}{T_1}\right). \quad (1)$$

The parameter A describes the equilibrium magnetization, parameter B the initial effects of the RF preparation pulse, and t is the time elapsed since the magnetization preparation pulse. The variable "t" is traditionally labeled as TI for inversion and TS for saturation—prepared measurements. Equation (1) provides the standard basis for T_1 estimation, which involves measuring a quantity proportional to the longitudinal magnetization component at various time points after the RF preparation pulse in order to fit the parameters to the observed data. Given that MR relies on relatively small signals, the inversion preparation has traditionally been used to obtain the widest signal range, which improves the robustness of the T1 estimate. With the exception of the perfect saturation, the accuracy of T1 estimation can be affected by the spin history from prior measurements. For the magnetization to return to 99% of its equilibrium value after an inversion, requires a time on the order of 4–5 × T1. The physiological range of native T1 values is on the order of seconds, and the accurate measurement of native T1's therefore requires a time on the order of minutes, using the early spectroscopic techniques [2]. Scaling this up to an imaging study with ~200 phase-encoding steps can add up to hours, which is impractical for phantoms and not feasible for in-vivo applications. Thus methods were required for acceleration [5].

Segmented look-locker T1 imaging

An approach for speeding up T1 measurements was developed by Look and Locker [6] long before MRI was introduced. With addition of k-space segmentation the eponymous technique allows T1 imaging that is sufficiently fast [7, 8] to fit within a tolerable breath-hold duration. A train of low flip angle gradient-echo read-outs, or read-outs during steady state precession, after an inversion pulse (Fig. 1a–b) was the most common form of Look-Locker imaging of the heart [9, 10]. The images are reconstructed from multiple k-space segments, each acquired during a different heart-beat and at a pre-defined time-point after inversion (i.e. TI value). This approach gives relative high temporal resolution for TI, but reconstructed images fall into different cardiac phases, resulting in a cine sequence of IR weighted frames (Fig. 1c–f). Equation 1 assumes that one and the same pixel location is sampled for different TI values. The Look-Locker technique works well for static pixels, but measuring the T1 of moving tissues, such as in the left ventricular wall requires tracking the relevant tissue across images (Fig. 1g). For cardiac applications of the Look-Locker technique, T1 was therefore generally only quantified for myocardial segments, rather than particular pixels within the myocardium, as the former can be tracked more easily than a single pixel location. The TI range in Look-Locker acquisitions is typically limited to 1–2 heart-beats, and k-space segment weighting can vary somewhat depending on the spin history preceding each inversion pulses, e.g. due to incomplete relaxation of longitudinal magnetization. Some of these aspects are illustrated in Fig. 1c, h. The segmented acquisition can lead to the usual subtle ghosting in case of arrhythmias and missed R-wave triggers [11]; artifacts related to the long T1's have also been reported [10].

A characteristic feature of all Look-locker acquisitions is that the M_z recovery is affected by the train of RF pulses applied for data-readouts. The recovery follows an effective T1* that is shorter than T1, and M_z recovers towards an equilibrium state with A < fully relaxed M_z, i.e. lower than for the undisturbed inversion recovery. The extent of readout saturation depends on readout type, flip angle, and repetition rate [9]. T1 can be recovered from T1* using an approximation originally proposed for fast, low angle "shot" (FLASH) image readouts with inversion preparation [12]:

$$T_1 = T_1^* \cdot \left(\frac{B}{A} - 1\right) \quad (2)$$

where A, and B correspond to the equally-named parameters in Eq. (1).

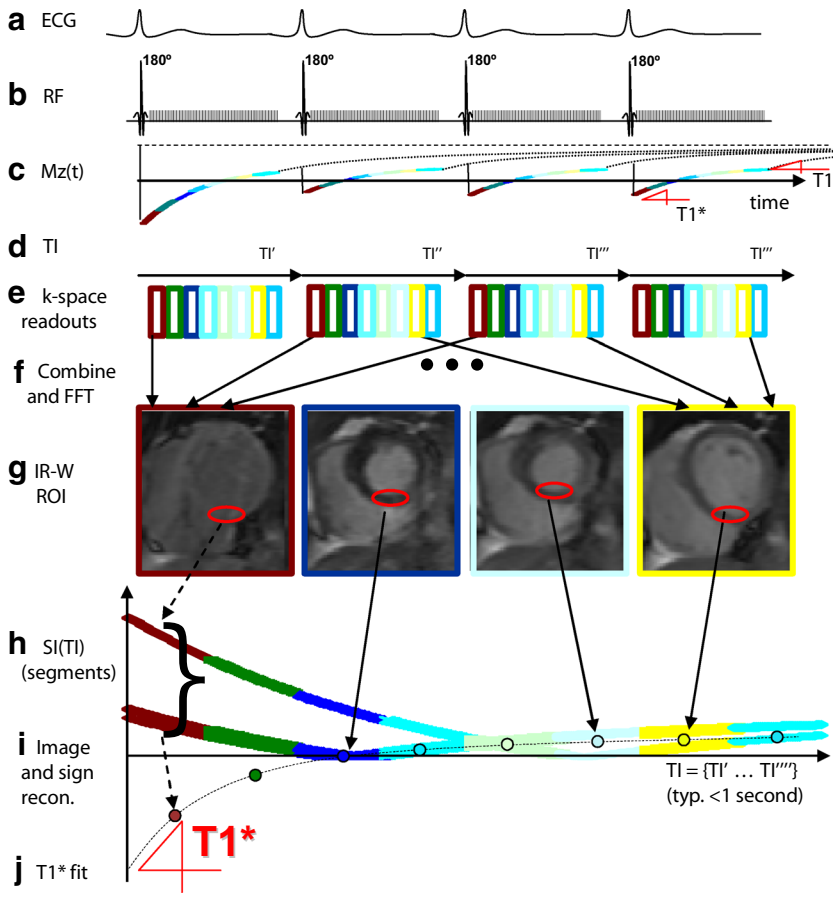

Fig. 1 Illustration of T1 measurement using prospectively triggered segmented Look-Locker sequence with indication of its limitations. **a** ECG signal to trigger. **b** RF 180° inversion pulses followed by small-angle readout pulses. **c** Evolution of the longitudinal magnetization (in static tissue) over several heart beats. *Solid lines* correspond to LL-accelerated recovery governed by the effective T1* relaxation time due to the influence of the read-out pulses. *Dotted lines* demonstrate the natural unobserved and undisturbed evolution of M_z. **d** Effective inversion times within each heart beat. **e** Readout segmentation method for accrual of adequate k-space for each TI. **f** Combining and reconstruction of **g** Inversion-recovery-weighted cine images. *Red circles* indicate motion of myocardial wall between images that requires correct tracking of the image intensity. **h** Calculation of image signal intensity (SI) involves combination of several k-space segments [*colored rectangles* in (**e**)] with similar TIs but slightly different spin history accrued between heart beats: bracket shown for the first SI(TI) only. **i** This results in magnetization magnitude samples as discrete points representing SI(TI) in each pixel, and requiring polarity restoration before fitting to Eq. 1. **j** T_1* (represented as the initial slope of the exponential recovery) is fitted to the observed relationship by non-linear optimization algorithms

T1 mapping using fast single shot image acquisitions

With advances in MR imaging acceleration it has become possible to acquire in a single shot a high resolution image, that is relatively unaffected by cardiac motion. "Single shot" means that all phase-encoding steps are carried out in rapid succession without interruption, typically taking 100–200 ms per image. With an adequate magnetization preparation, this single-shot approach has been proposed to sample M_z relaxation. For T1 mapping, multiple images are acquired within a single breath-hold at pre-designated cardiac delay times to freeze cardiac motion [13]. In order to improve the SNR and minimize disturbance of the inversion recovery, the image read-outs are based on steady-state free precession. This ground-breaking work by Messroghli et al. [13] led to the most successful clinical T1 mapping approaches currently used, enhanced by further optimized read-out schemes, and also pointed to the potential of using a saturation preparation to limit the heart-rate dependencies in the measured T1.

Modified look locker inversion recovery (original MOLLI)

Messroghli et al. developed a framework for the Modified Look-Locker Imaging (MOLLI) family of techniques [14],

followed by technical optimization of various acquisition parameters [15], and first applications in patients [15]. The original MOLLI acquisition principles are presented in Fig. 2. Briefly, there are three inversion preparations which shift the inversion pulses by a pre-set amount relative to the single shot image acquisitions at a fixed time in the cardiac cycle, that follow each inversion pulse (Fig. 1a, b). Each group of inversion pulse, image read-outs, and rest period for relaxation recovery is termed a Look-Locker cycle. The MOLLI scheme shown in Fig. 2 is referred two as a 3(3)-3(3)-5 scheme, because the Look-Locker cycles involve in the order shown in Fig. 2, acquisition of 3, 3, and 5 images after each inversion, separated by three heart-beat long unperturbed recovery epochs after the first and second inversions. Figure 2c, e demonstrates that the magnetization undergoes rapid changes during the readouts, and an undisturbed relaxation recovery governed by T1 between readouts. The relatively long unperturbed recovery periods after each Look-Locker cycle allow M_z to return to equilibrium before the next inversion recovery cycle. This permits to combine the acquired data into a *single* inversion recovery curve with an effective relaxation constant T1* (Fig. 2e). MOLLI uses SSFP readouts with relatively large flip angles (50° originally) [14]. Given the relative sparsity of image acquisitions between heartbeats (and ramp up and down pulses, not shown for simplicity) the effective $T1^*_{MOLLI}$ is only moderately shorter than T1, which allows relatively accurate correction using Eq. 2, even though Eq. 2 was proposed for much lower flip angle FLASH acquisitions [14, 16, 17]. In contrast to LL experiments, the images of the heart appear frozen in a single cardiac phase (Fig. 2d). The downside is that the data acquisition underlying each image extends for a relatively long period of the heart cycle, (Fig. 2b). IR weighting in k-space (Fig. 2c, e, colored lines) covers a relatively wide TI range, i.e. using a single TI for each image as suggested by Eq. 1 is an approximation, in

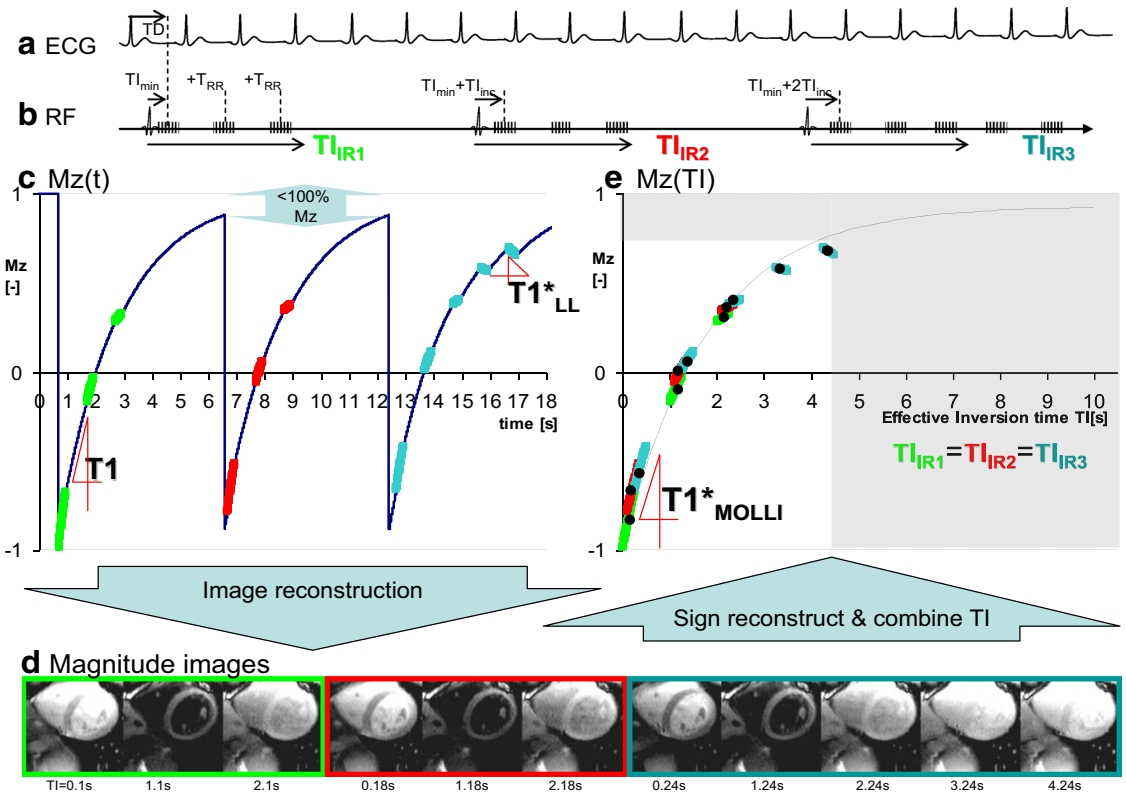

Fig. 2 The original single breath-hold Modified Look Locker Inversion recovery (MOLLI) acquisition with a scheme involving three magnetization inversions. **a** ECG triggers for freezing image acquisition at a preset cardiac delay TD time. **b** Inversion preparations define three experiments ("Look-Locker cycles"). Images are acquired at inversion times starting from a preset TI_{min} and incremented by RR-interval within each experiment. TI values are offset by TI_{inc} between experiments. Each experiment is followed by a relatively long pause. **c** M_z evolution is a combination of unobserved free recovery (T1), and Look-Locker conditions much shorter $T1^*_{LL}$ and lower equilibrium ("A" in Eq. 1, hence the recovery may be directed counter-intuitively downwards, as shown). Note that for long T1, M_z may not return to equilibrium ($M_z < 100\%$) before an inversion. **d** Reconstructed magnitude images. **e** Fitting of individual pixel data into the MOLLI effective relaxation time T1*. For each pixel only one value of intensity is used (*Black circles*). Each individual point arises from a transformation of k-space signal trajectories of M_z recovery during the relatively long acquisition of each *single shot*, high resolution image

particular for shorter TI's. Figure 2c also demonstrates that for longer T1, or higher heart rates, the three heart-beat recovery epochs are not necessarily adequate for M_z to fully return to its equilibrium state, so that the 2nd and 3rd inversion experiments start with a progressively larger bias to underestimate the parameter B in Eq. 1. This causes small misalignments between the fitted data (Fig. 2e), the main source of the heart-rate dependent underestimation for longer T1's [15, 18, 19]. The large-flip angle readouts were later decreased to 35° [15, 20], which may in good part be due to factors unrelated to the Deichmann-Haase correction, and instead to effects like magnetization transfer (MT; see below for details on MT effects on T1). The downside of the original 3(3)-3(3)-5 MOLLI scheme is the relatively long breath-hold, with the longest Look-Locker cycle at the end, which may contribute to its reported sensitivity to patient motion [21].

Short variants of MOLLI and their tradeoffs

Eventually the problem with long breath holds was addressed [18] and multiple shortened versions of MOLLI offering various trade-offs followed soon [19, 22]. Shortened MOLLI (ShMOLLI) introduced the idea of acquiring most samples at the beginning of the breath hold (front-loading), and of reducing the acquisition time by a deliberate choice of short recovery periods that are inadequate for longer T1's. The effects of overly short recovery periods for longer T1's are bypassed with ShMOLLI by a conditional reconstruction algorithm to choose only samples for the reconstruction [18] such that T1 can be estimated without bias from sub-optimally recovered data. Reducing the breath hold duration seems to compensate for the lower sample number, with the added benefit of a relatively accurate estimation of T1, independent of the heart rate [18]. For native T1 estimation, ShMOLLI relies mostly on the first 5 samples, and conditional processing will remove any subsequent samples that do not adequately fit Eq. 1. However, as illustrated in Fig. 3, ShMOLLI lacks the significant data redundancy inherent in the use of multiple longer Look-Locker cycles, which makes ShMOLLI more sensitive to missed ECG-triggers, in particular when the 2nd trigger signal (ECG signal for 2nd Look-Locker cycle) is missed (Fig. 3a).

An alternative proposal to shorten the acquisition was to remove one of the Look-Locker cycles from the original MOLLI scheme resulting in a shorter 3(3)-5 scheme, an approach introduced in the so-called "11-hb MOLLI" [19], where "hb" stands for "heart beat". The shorter 11-hb MOLLI technique is characterized by similar dependencies on T1 and heart rate as the original 17-hb MOLLI scheme [19]. Front loading (i.e. using a 5(3)-3, instead of a 3(3)-5 scheme) was proposed shortly afterwards to reduce heart rate dependency [23]. Reducing the number of short TI samples however has a negative impact on the estimation of shorter T1's, as illustrated in Fig. 4. This problem was addressed by keeping the number of Look-Locker cycles at 3 as in the original MOLLI scheme, but reducing the number of samples in the Look-Locker cycles and shortening the rest period in some Look-Locker cycles. This was first implemented as a 12-hb, back-loaded 2(2)-2(2)-4 MOLLI variant [22], and followed shortly thereafter by another 11-hb front-loaded 4(1)-3(1)-2 MOLLI variant [24]. The two MOLLI schemes have recovery periods as

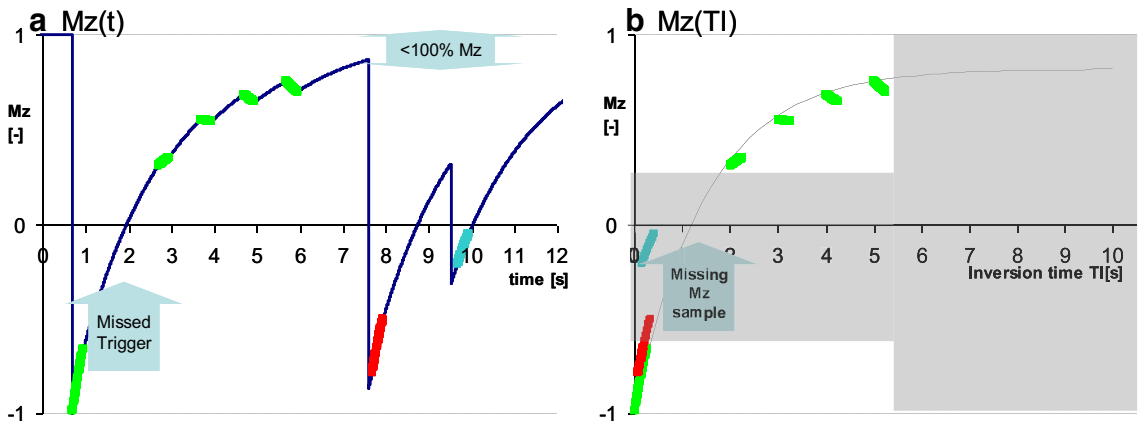

Fig. 3 Shortened Modified Look-Locker Inversion recovery (ShMOLLI). **a** evolution of longitudinal magnetization M_z demonstrating the implications of a missed trigger in the second heart beat. **b** data used for conditional fitting demonstrate areas where M_z is sampled sub-optimally (*grey areas*). Lack of data from the second heart beat range affects robustness of estimates and may lead to erroneous inclusion of 2nd heart-beat data into reconstruction resulting in artificial underestimation of T1. Advice is to optimize ECG signal quality, listen to regular acquisition pattern and check fit quality maps. *Conditions* are exaggerated to make the effects visible to the naked eye

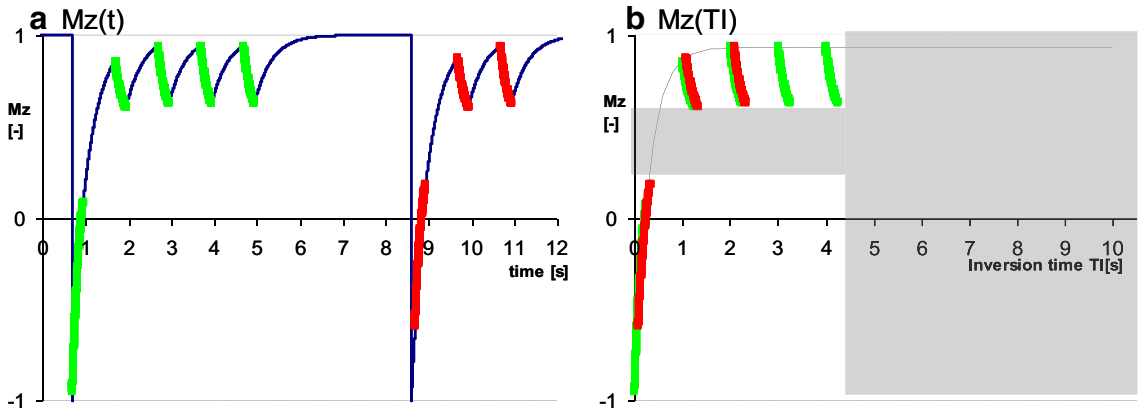

Fig. 4 Modern front-loaded 5(3)-3 MOLLI variant for native T1 mapping. **a** evolution of M_z for very short T1 and **b** fitting T1* demonstrates the relative lack of information for short T1 (*gray shaded area*) and unnecessary over sampling of long TI range, which make the variant sub-optimal to study post-contrast conditions and short T1 species such as fat. *Conditions* are exaggerated to make the effects obvious to the naked eye

short as ShMOLLI, but were proposed without the conditional reconstruction that prevents underestimation of long T1's (Fig. 5). Potentially, the conditional reconstruction can be applied to other shortened MOLLI schemes pending careful optimization. Currently, care needs to be taken to avoid inadvertent application of any MOLLI variant optimized for *post-contrast* measurement of shorter T1's to measurements of longer (native) T1's. For any post-contrast interpretation of T1 in some structures, such as cysts, one may also need to take into account that contrast delivery was severely restricted, T1 still relatively long after contrast injection, and therefore one needs to check that the MOLLI variant used does not introduce a bias to underestimate those longer T1's.

Saturation prepared T1 mapping

While T1 mapping is possible with any preparation pulse [7], using a perfect saturation pulse has the distinct advantage of resetting the spin-relaxation history, i.e. creating a magnetization state that is independent of any prior magnetization evolution. The saturation preparation was recognized early on as a way of limiting heart-dependence in T1 estimates [13]. The flexibility of this approach was demonstrated first by Song et al. [25], followed by a practical implementation suitable for clinical applications under the name of SAturation recovery single-SHot Acquisition (SASHA) [26]. In contrast to MOLLI, SASHA demonstrates less sensitivity to heart rate, magnetization transfer effects, and myocardial T2

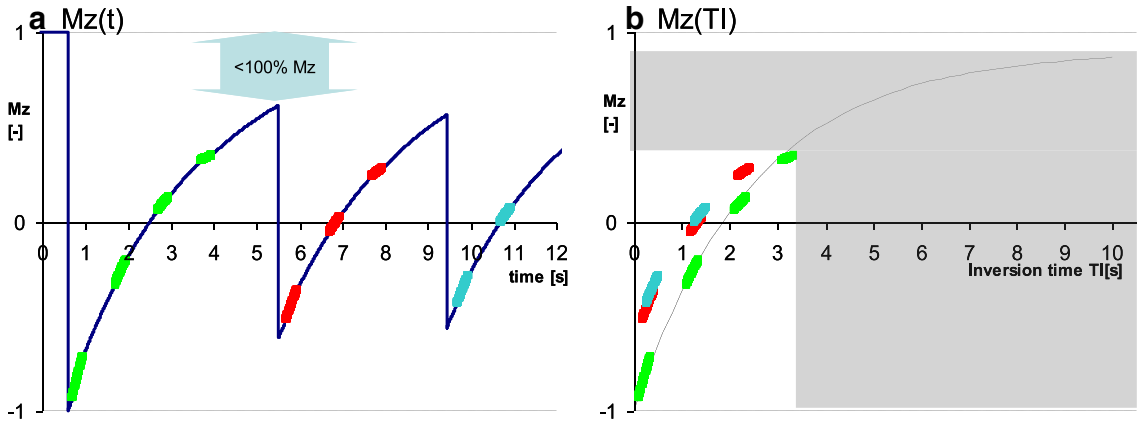

Fig. 5 Modern front-loaded 4(1)-3(1)-2 MOLLI variant for post-contrast T1 mapping. **a** evolution of M_z for long T1 species demonstrates the narrower range of inversion times and potentially large effects of sub optimally short recovery periods. **b** fitting T1* shows poor overlap between the data from first and the subsequent IR experiments underlying potentially severe T1 underestimation for long T1 species, which may affect tissues that take up contrast slowly or not at all (e.g. microvascular obstruction and cysts, or when applied by mistake in pre-contrast settings). *Conditions* are exaggerated to make the effects obvious to the naked eye

[26, 27]. The original paper thoroughly discussed the errors arising from breaching assumptions of perfect saturation and noise-free image acquisition, with much ongoing work continuing to address practical imperfections of SASHA and their impact [28–30]. Practical comparisons indicate that SASHA produces higher but less precise T1 estimates than MOLLI [31–33]. Recent experimental evidence confirms the relatively small T2- and magnetization-transfer-related errors for SASHA T1 estimates in comparison to T1 measured with IR-TSE in ex-vivo heart tissue [34]. Figure 6 demonstrates the compounding effects of suboptimal saturation and irregular ECG triggering.

Facts and myths in the interpretation of T1 measurements

Longitudinal magnetization relaxation mechanisms in native T1

T1 as a single relaxation parameter is adequate for most uniform materials where all MR visible nuclei tumble in a manner that can be characterized by similar correlation times [35]. Under these conditions, the BPP (Bluembergen-Purcell-Pound) theory explains well the temperature and frequency dependencies of the relaxation times in fluids of various viscosity up to the point where they become solids. But BPP theory has long been recognized as inadequate for even simple macromolecular solutions that exhibit compartmentalization of molecular pools visible to MR [36]. Living human tissue is characterized by even more complex interactions involving multiple scales of chemical, structural and functional detail, with each subunit characterized by its own molecular milieu and respective range of relaxation times. As such, both theory and modern NMR relaxation experiments can directly reveal the presence of multiple tissue sub-spaces with characteristic T1/T2 relaxation time combinations, that all change in response to physiological derangements [37]. This precludes defining any particular in-vivo T1 relaxation time estimate as an inherently accurate representation of the underlying relaxation process, but instead suggests that different T1 measurement techniques provide different views of the underlying relaxation processes.

Native T1: effects of magnetization transfer and vascular state

Prior studies of 1H relaxation in collagen rich cartilage provide some valuable insights for the interpretation of myocardial T1 as a measure of interstitial fibrosis. Dense tissue components, such as collagen, have extremely short T2 relaxation times (≪1 ms), which means that the pool of spins bound to collagen fibers is not detected by standard imaging sequences, except those dedicated to ultra-short echo-time (UTE) imaging [38]. Nevertheless, this "dark" (i.e. generally not MR visible) pool of spins, can still exert a powerful effect on the relaxation of more mobile 1H spins that contribute to the measured MR signal through the transfer of magnetization from one pool to the other (e.g. through magnetic dipole interactions). The magnitude of magnetization transfer effects depends on the amount of radio-frequency power received by the dark pool of spins (with a relatively very broad distribution of resonance frequencies, alas a very short T2), the size of the dark-spin pool, and

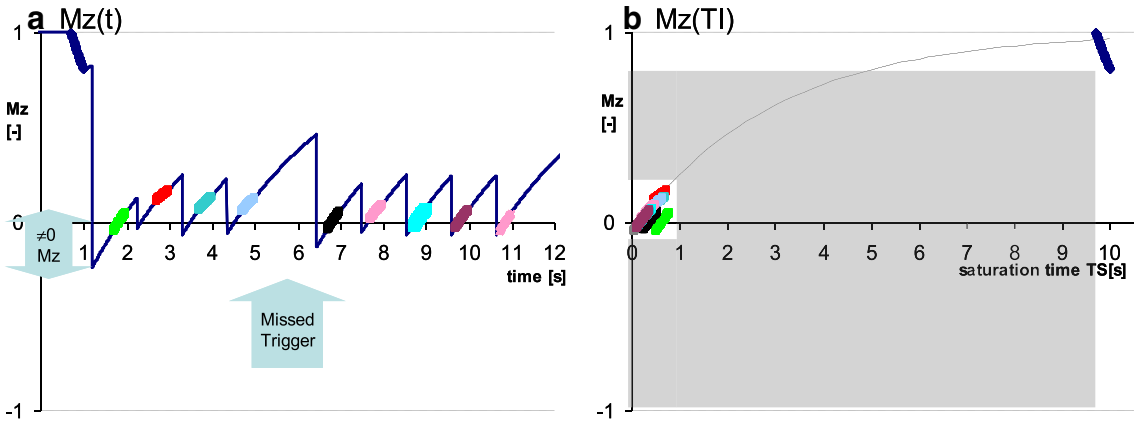

Fig. 6 Demonstration of the impact of imperfect saturation combined with mis-triggering on the data consistency underlying saturation recovery single-shot acquisition (SASHA) T1 mapping. **a** Evolution of longitudinal magnetization shows a loss of the regular pattern with decreasing saturation time between the heartbeats when saturation pulse flip angle exceeds the nominal 90°. **b** Attempt to align the data against common saturation time demonstrates significant deviation of the sample after first saturation (*green*) and after the lost trigger (*black*) from the expected recovery curve. Relatively *large area shaded in gray* indicate that SASHA samples a relatively limited range of the M_z recovery compared with MOLLI variants (Figs. 2, 3, 4, 5). *Conditions* are exaggerated to make the effects visible to the naked eye

the strength of the nuclear-spin energy coupling underpinning the MT. Both constituent macromolecules and collagen lead to MT effects in cartiladge [39]. Along with the above-mentioned departures from BPP theory [36], the direct study of collagen indicates that water content has similar effects on T1 and T2 [37, 40]. Thus, it is not realistic to expect that sequences for native T1 mapping can readily quantify interstitial fibrosis, without confounding by other factors.

It is likely that observed in-vivo T1 *increases* are linked to a proxy effect of fluid accumulation in fibrotic tissue, a process shared with many other pathologies such as infarction. Recent research also reveals the important role of water in the intravascular space on tissue T1, which can change with vascular tone and vasodilation [41]. MOLLI techniques also show sensitivity to T2 [27], which may cause some blood-oxygen-level-dependent (BOLD) changes to T1 under adenosine stress [42–44]. Conversely, for high interstitial protein or paramagnetic content overloading conditions characterizing states with lower native T1, such as Fabry's disease and tissue iron overload, concurrently lower T2 values and a stronger MT may further enhance the pathological decrease of native T1 measured by MOLLI, and in particular in the presence of readout saturation effects and inversion pulse deficiencies [30].

Post-contrast T1 mapping and extracellular volume quantification

Contrast administration is one of the major tools to selectively manipulate the relaxation times and provides the basis for some of the most ubiquitous CMR techniques [45]. In the case of simple fluids, the addition of contrast agents is easiest to understand using the R1 relaxation rate, an inverse of the relaxation time, and the concept of contrast-relaxivity. In terms of relaxation rate, the effect of a contrast agent on R1 can be expressed as a linear function of concentration [C] with the contrast relaxivity $r_{1\text{contrast}}$ as linear coefficient:

$$R_1 = {}^1/_{T_1} = R_{1native} + r_{1contrast} \times [C]. \tag{3}$$

The initial interest in cardiac T1 mapping was to a considerable degree motivated by the goal of detecting changes in the extracellular volume fraction. It is well documented that in diseases such as aortic stenosis, the pressure overload of the left ventricle leads to a build-up of connective tissue in the interstitial space and an expansion of the extra-cellular volume (ECV) fraction, with biopsy findings correlating with ECV measures [5, 46]. In this context, it is useful to emphasize that the ECV fraction does not increase as a result of the cardiomyocyte hypertrophy alone. The process of physiological hypertrophy, e.g. hypertrophy associated with the normal growth of the heart does not lead to interstitial fibrosis, and consequently the ECV—a volume fraction—does not change significantly between adolescence and early adulthood. In contrast, pathological hypertrophy is associated with interstitial fibrosis, and capillary rarefication which leads to a shift in balance between extra- and intra-cellular volumes, and an increase of the ECV fraction. In mouse models of LV pressure overload, the initial response of the myocardium manifests itself by an increase of cardiomyocyte size, without a significant increase of ECV, and only when the pressure overload leads to the built-up of connective tissue in the interstitial space does ECV increase significantly [47]. The complement of ECV, namely 1-ECV, which corresponds to the intra-cellular volume fraction, is by itself not a good marker of cardiomyocyte hypertrophy, though the product of (1-ECV) with LV mass can be used to assess changes of cardiomyocyte volume in the LV.

Many MR contrast agents are extra-cellular contrast agents to limit their potentially toxic effects, and the volume of distribution of these contrast agents can therefore serve as a measure of the ECV fraction. If one assumes that the contrast agent reaches a uniform distribution in the extra-cellular space, then it is possible to estimate the extra-cellular volume fraction from the change in myocardial R1 between a pre-contrast measurement and a post-contrast measurement. This myocardial R1 difference is normalized by the change of R1 in blood, as the latter serves as a reference with a volume of distribution that corresponds to 1 minus the blood hematocrit (*Hct*) fraction. This leads to the standard definition of ECV that is used in CMR to quantify the extra-cellular volume fraction from pre- and post-contrast T1 measurements in blood and myocardium.

$$(1 - Hct) \cdot \frac{\Delta R_1(tissue)}{\Delta R_1(blood)} = \lambda_{Gd} \cdot (1 - Hct) = ECV. \tag{4}$$

The respective relaxation rate changes in the numerator and denominator of Eq. (4) may depend on the technique used to measure them, predictably resulting in differences in the derived ECV, e.g. between MOLLI and SASHA [48].

The derivation of Eq. (4) for ECV assumes that Gd concentration is in equilibrium between compartments marked by thick dashed outline in Fig. 7. It also assumes that mobile 1H nuclei are exchanging rapidly between the intra- and extra-cellular spaces, as the tissue relaxation rate is then a linear function of the blood R1. The qualifier of "rapid" for the water exchange refers to the rate of water exchange relative to the difference in intrinsic R1's between interstitial and intra-cellular spaces. This means that by increasing this difference in intrinsic R1 rates by administration of contrast one can move from the fast exchange through the intermediate, to the slow

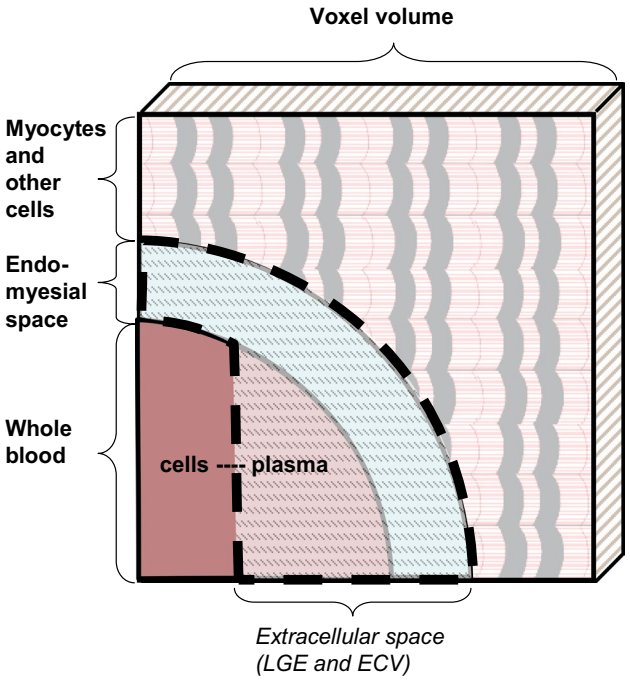

Fig. 7 Simplified model of the compartments carrying the Gd-contrast used for LGE and ECV estimation. Note that the intra-myocardial blood pool plasma is integral part of LGE contrast and ECV measurements (*dashed outline*), which are thus expected to be sensitive to vasoreactive challenges

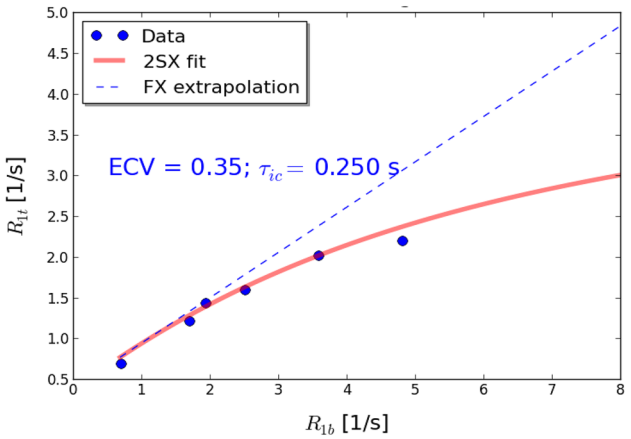

Fig. 8 The R1 relaxation rate in myocardial tissue increases linearly as a function of the simultaneously measured R1 relaxation rate in blood if conditions of fast 1H exchange across the cardiomyocyte membrane apply. Fast exchange (FX) conditions apply when the difference between the intrinsic extra- and intra-cellular relaxation rates is small compared to the 1H exchange rate, i.e. at lower contrast Gd contrast concentrations in blood. Under these conditions the relaxation rate in tissue increases approximately linear with the concentration R1 relaxation rate of blood (*dashed line*), with the slope giving the partition coefficient for Gd in myocardial tissue, a prerequisite for ECV. At higher contrast concentrations the R1 relaxation rate of tissue shows a sub-linear dependence on R1 in blood, with the deviation from the *dashed line* (for fast exchange limit) becoming a function of the exchange rate, or the intra-cellular lifetime of water. The data shown in the graph were acquired in a mouse model of pressure overload and show a significant increase of the intra-cellular lifetime to 250 ms, above its normal range, as a result of cardiomyocyte hypertrophy

exchange regime. In this latter case, the myocardial R1 no longer changes linearly with the R1 measured in blood (as surrogate marker for the plasma R1 in the tissue), and the rate of exchange of water between the interstitial and intra-cellular spaces becomes the effective bottleneck for increases in the tissue relaxation rate. The resulting sub-linear dependence of R1 in tissue on the plasma R1 can result in an underestimate of ECV. In addition, analysis of the sub-linear dependence of the tissue R1 can be used to estimate the rate of water exchange, which is a surrogate marker of cardiomyocyte size [47]. The effect of the water exchange rate for the dependence of the myocardial R1 on the R1 of blood is illustrated in Fig. 8.

The possible effects of water exchange mean that the application of the method embodied by Eq. (4) for estimating ECV should use post-contrast T1 measurements where conditions of fast-exchange between intra- and extra-cellular spaces apply. Otherwise, the myocardial relaxation rate R1 will be lower than predicted by the fast-exchange model, and in practice this means that ECV is underestimated. Of note, the conditions of fast-exchange are most likely not to apply after contrast administration with increasing cardiomyocyte size, meaning that ECV is more likely to be underestimated in case of ventricular hypertrophy, compared to normal conditions [49]. A delay of ~15 min after injection of single-dosage of Gd-contrast is generally sufficient for getting a measure of ECV that is unlikely to be affected by slower than expected ^{1}H exchange [1]. Based on what can be inferred from compartmental tracer-kinetic models used for analysis of first pass perfusion studies, one can expect that the contrast-concentrations equilibrate between the extra- and intra-cellular spaces in viable myocardium within 3–4 min after contrast injection. The condition of being in the fast-exchange limit is therefore the more demanding one in terms of the required delay between a single-dose contrast injection and the post-contrast T1 measurements used for estimating ECV with Eq. (2). Still, it is also possible to fit the relation between myocardial R1 and blood R1 with a model that considers the rate of 1H exchange, though it is more complex than (2), and requires at least three post-contrast T1 measurements to determine the unknown model parameters including the intra-cellular lifetime of water [47].

The finding that native T1 reflects the myocardial vasodilator state led to the realization that stress would also affect ECV [41], with early evidence showing a moderate-strength correlation between ΔT_1 (change for native T1) and the change of ECV between rest and stress, respectively [50]. The authors attributed the increase of the extra-cellular

volume fraction between rest and hyperemia to an increase of myocardial blood volume, which contributes to the extracellular volume fraction. Any discussion of such points needs caution, as the simple two-compartmental blood model in Fig. 7 represents a drastic simplification, and the interpretation of ECV generally neglects the recognized dependencies of hematocrit [51], and vascular reactivity [52] on the vessel-size.

Synthetic ECV

An estimation of ECV based on Eq. (4) requires that the blood hematocrit be known. Though the administration of contrast already creates the need for intravenous access, obtaining a blood sample and determining hematocrit (*Hct*) imposes an additional burden. An alternative approach, proposed by Treibel et al. [33] is based on estimating *Hct* from the pre-contrast T1 of arterial blood. In a two-compartment model with fast exchange of water between plasma and cytoplasm, the R1 of the whole blood can be described as weighted average of the R1's for erythrocytes and plasma, where the erythrocyte fraction is a function of the blood hematocrit [53]. The resulting relationship between blood R_1 and *Hct* is well approximated by a linear equation: $R_1 = a \cdot Hct + b$, where a and b are empirical constants that vary by field strength and sequence type [53]. Treibel et al. inverted this relationship and used it to predict *Hct* from the measured native blood R1. The estimate of ECV obtained with this blood-T1-based estimate of *Hct* is now commonly referred to as "synthetic ECV". Treibel et al. found that synthetic ECV correlates well with conventional ECV, without introducing a bias. The calibration equations derived by Treibel et al. for T1 measurements with MOLLI and shMOLLI at 1.5 T also predict the observed differences of ~100 ms in T1 between male and female adults [54] using average hematocrits of 0.41 and 0.38 respectively. As a note of caution, it should be pointed out that different equations are presented in this work for two selected MOLLI variants (Siemens MOLLI and ShMOLLI). Indeed, slight variations between MOLLI techniques may be a reason why recent small independent validations show relatively poor performance for the individual Hct estimates, even though average Hct and ECV are less affected [55–58].

Summary and conclusions

Myocardial T1 mapping has emerged in the last few years as a powerful approach to myocardial tissue characterization. Native T1 and myocardial ECV have been validated as robust biomarkers in numerous cardiac pathologies, and may provide unique advantages for non-invasive therapy monitoring. This overview includes a summary of pitfalls and gaps in the understanding of the physical and physiological mechanisms underlying the interpretation and accuracy of any practical measurement. Still, the lack of a comprehensive pathophysiological mechanistic framework should not be considered a barrier to the ongoing clinical translation of selected methods positively validated for their sensitivity to disease.

Funding SKP is supported by the NIHR Biomedical Research Centre, Oxford. The views expressed are those of the author(s) and not necessarily those of the NHS, the NIHR or the Department of Health.

Compliance with ethical standards

Conflict of interest SKP has authorship rights for US Patent US20120078084: SYSTEMS AND METHODS FOR SHORTENED LOOK LOCKER INVERSION RECOVERY (Sh-MOLLI) CARDIAC GATED MAPPING OF T1. September 29, 2010. Patent is managed by Oxford University Innovations, All rights transferred exclusively to Siemens Medical. MJH has no potential conflicts of interests to disclose in relation to this manuscript.

Research involving with human and animal participants This review article does not report on unpublished studies that involved human subjects or animals.

References

1. Moon JC, Messroghli DR, Kellman P, Piechnik SK, Robson MD, Ugander M, Gatehouse PD, Arai AE, Friedrich MG, Neubauer S, Schulz-Menger J, Schelbert EB (2013) Myocardial T1 mapping and extracellular volume quantification: a Society for Cardiovascular Magnetic Resonance (SCMR) and CMR Working Group of the European Society of Cardiology consensus statement. J Cardiovasc Magn Reson 15:92
2. Williams ES, Kaplan JI, Thatcher F (1980) Prolongation of proton spin lattice relaxation times in regionally ischemic tissue from dog hearts. J Nucl Med 21(5):449–453
3. Higgins CB, Herfkens R, Lipton MJ, Sievers R, Sheldon P, Kaufman L, Crooks LE (1983) Nuclear magnetic resonance imaging of acute myocardial infarction in dogs: alterations in magnetic relaxation times. Am J Cardiol 52(1):184–188
4. Wesbey GE, Higgins CB, McNamara MT, Engelstad BL, Lipton MJ, Sievers R, Ehman RL, Lovin J, Brasch RC (1984) Effect of gadolinium-DTPA on the magnetic relaxation times of normal and infarcted myocardium. Radiology 153(1):165–169
5. Fontana M, White SK, Banypersad SM, Sado DM, Maestrini V, Flett AS, Piechnik SK, Neubauer S, Roberts N, Moon JC (2012) Comparison of T1 mapping techniques for ECV quantification. Histological validation and reproducibility of ShMOLLI versus multibreath-hold T1 quantification equilibrium contrast CMR. J Cardiovasc Magn Reson 14:88
6. Look D, Locker D (1970) Time saving in measurement of NMR and EPR relaxation times. Rev Sci Instrum 41(2):250–251
7. Brix G, Schad LR, Deimling M, Lorenz WJ (1990) Fast and precise T1 imaging using a TOMROP sequence. Magn Reson Imaging 8(4):351–356
8. Haase A, Matthaei D, Bartkowski R, Duhmke E, Leibfritz D (1989) Inversion recovery snapshot FLASH MR imaging. J Comput Assist Tomogr 13(6):1036–1040

9. Scheffler K, Hennig J (2001) T1 quantification with inversion recovery TrueFISP. Magn Reson Med 45(4):720–723
10. Goldfarb JW, Arnold S, Schapiro W, Reichek N (2005) On the cause of spatial displacement of long T1 species in segmented inversion recovery prepared imaging. Magn Reson Med 54(2):481–485
11. Ferreira PF, Gatehouse PD, Mohiaddin RH, Firmin DN (2013) Cardiovascular magnetic resonance artefacts. J Cardiovasc Magn Reson 15:41
12. Deichmann R, Haase A (1992) Quantification of T1 values by snapshot-flash NMR imaging. J Magn Reson 96(3):608–612
13. Messroghli DR, Niendorf T, Schulz-Menger J, Dietz R, Friedrich MG (2003) T1 mapping in patients with acute myocardial infarction. J Cardiovasc Magn Reson 5(2):353–359
14. Messroghli DR, Radjenovic A, Kozerke S, Higgins DM, Sivananthan MU, Ridgway JP (2004) Modified Look-Locker inversion recovery (MOLLI) for high-resolution T1 mapping of the heart. Magn Reson Med 52(1):141–146
15. Messroghli DR, Greiser A, Fröhlich M, Dietz R, Schulz-Menger J (2007) Optimization and validation of a fully-integrated pulse sequence for modified look-locker inversion-recovery (MOLLI) T1 mapping of the heart. J Magn Reson Imaging 26(4):1081–1086
16. Deichmann R, Adolf H, Noth U, Morrissey S, Schwarzbauer C, Haase A (1995) Fast T2-mapping with snapshot flash imaging. Magn Reson Imaging 13(4):633–639
17. Rodgers CT, Piechnik SK, Delabarre LJ, Van de Moortele PF, Snyder CJ, Neubauer S, Robson MD, Vaughan JT (2012) Inversion recovery at 7T in the human myocardium: measurement of T(1), inversion efficiency and B(1)(+). Magn Reson Med 70(4):1038–1046
18. Piechnik SK, Ferreira VM, Dall'Armellina E, Cochlin LE, Greiser A, Neubauer S, Robson MD (2010) Shortened modified Look-Locker inversion recovery (ShMOLLI) for clinical myocardial T1-mapping at 1.5 and 3 T within a 9 heartbeat breathhold. J Cardiovasc Magn Reson 12:69
19. Lee JJ, Liu S, Nacif MS, Ugander M, Han J, Kawel N, Sibley CT, Kellman P, Arai AE, Bluemke DA (2011) Myocardial T1 and extracellular volume fraction mapping at 3T. J Cardiovasc Magn Reson 13:75
20. Gai ND, Stehning C, Nacif M, Bluemke DA (2013) Modified Look-Locker T1 evaluation using Bloch simulations: human and phantom validation. Magn Reson Med 69(2):329–336
21. Messroghli DR, Plein S, Higgins DM, Walters K, Jones TR, Ridgway JP, Sivananthan MU (2006) Human myocardium: single-breath-hold MR T1 mapping with high spatial resolution—reproducibility study. Radiology 238(3):1004–1012
22. Salerno M (2013) Comparison of methods for determining the partition coefficient of gadolinium in the myocardium using T1 mapping. J Magn Reson Imaging 38(1):217–224
23. Kellman P, Wilson JR, Xue H, Ugander M, Arai AE (2012) Extracellular volume fraction mapping in the myocardium, part 1: evaluation of an automated method. J Cardiovasc Magn Reson 14:63
24. Kellman P, Arai AE, Xue H (2013) T1 and extracellular volume mapping in the heart: estimation of error maps and the influence of noise on precision. J Cardiovasc Magn Reson 15:56
25. Kawel N, Nacif M, Zavodni A, Jones J, Liu S, Sibley CT, Bluemke DA (2012) T1 mapping of the myocardium: intra-individual assessment of post-contrast T1 time evolution and extracellular volume fraction at 3 T for Gd-DTPA and Gd-BOPTA. J Cardiovasc Magn Reson 14:26
26. Chow K, Flewitt JA, Green JD, Pagano JJ, Friedrich MG, Thompson RB (2014) Saturation recovery single-shot acquisition (SASHA) for myocardial T(1) mapping. Magn Reson Med 71(6):2082–2095
27. Moon JC, Messroghli DR, Kellman P, Piechnik SK, Robson MD, Ugander M, Gatehouse PD, Arai AE, Friedrich MG, Neubauer S, Schulz-Menger J, Schelbert EB (2013) Myocardial T1 mapping and extracellular volume quantification: a Society for Cardiovascular Magnetic Resonance (SCMR) and CMR Working Group of the European Society of Cardiology consensus statement. J Cardiovasc Magn Reson 15(1):92
28. Chow K, Yang Y, Shaw P, Kramer CM, Salerno M (2016) Robust free-breathing SASHA T-1 mapping with high-contrast image registration. J Cardiovasc Magn Reson 18:47
29. Chow K, Kellman P, Spottiswoode BS, Nielles-Vallespin S, Arai AE, Salerno M, Thompson RB (2015) Saturation pulse design for quantitative myocardial T1 mapping. J Cardiovasc Magn Reson 17:84
30. Kellman P, Herzka DA, Hansen MS (2014) Adiabatic inversion pulses for myocardial T1 mapping. Magn Reson Med 71(4):1428–1434
31. Teixeira T, Hafyane T, Stikov N, Akdeniz C, Greiser A, Friedrich MG (2016) Comparison of different cardiovascular magnetic resonance sequences for native myocardial T1 mapping at 3 T. J Cardiovasc Magn Reson 18(1):65
32. Roujol S, Weingartner S, Foppa M, Chow K, Kawaji K, Ngo LH, Kellman P, Manning WJ, Thompson RB, Nezafat R (2014) Accuracy, precision, and reproducibility of four T1 mapping sequences: a head-to-head comparison of MOLLI, ShMOLLI, SASHA, and SAPPHIRE. Radiology 272(3):683–689
33. Treibel TA, Fontana M, Maestrini V, Castelletti S, Rosmini S, Simpson J, Nasis A, Bhuva AN, Bulluck H, Abdel-Gadir A, White SK, Manisty C, Spottiswoode BS, Wong TC, Piechnik SK, Kellman P, Robson MD, Schelbert EB, Moon JC (2016) Automatic measurement of the myocardial interstitium: synthetic extracellular volume quantification without hematocrit sampling. JACC Cardiovasc Imaging 9(1):54–63
34. Hafyane T, Duquette C, Mongeon FP, Cohen-Adad J, Stikov N (2017) Bringing the T1 mapping sequences together: a study of the T2 and magnetization transfer effects in ex vivo pig hearts. Paper presented at: 20th Annual SCMR Scientific Sessions, Washington, DC
35. Bloembergen NP, Purcell EM, Pound RV (1948) Relaxation effects in nuclear magnetic resonance absorption. Phys Rev 73:679–746
36. Fullerton GD (1992) Physiologic basis of magnetic relaxation. In: Stark DD, Bradley WG (eds) Magnetic Resonance Imaging. Vol1. 2nd ed. Mosby, St. Louis, London, pp 88–108
37. Gul ENF, Singh C, Papaioannou A, Sinha N, Boutis GS (2015) The behavior of water in collagen and hydroxyapatite sites of cortical bone: Fracture, mechanical wear, and load bearing studies. J Phys Chem C 119(37):21528–21537
38. Gatehouse PD, Bydder GM (2003) Magnetic resonance imaging of short T2 components in tissue. Clin Radiol 58(1):1–19
39. Gray ML, Burstein D, Lesperance LM, Gehrke L (1995) Magnetization transfer in cartilage and its constituent macromolecules. Magn Reson Med 34(3):319–325
40. Rodin VV (2005) [NMR-relaxation in hydrated collagen from the spotted dogfish]. Biofizika 50(2):223–230
41. Mahmod M, Piechnik SK, Levelt E, Ferreira VM, Francis JM, Lewis A, Pal N, Dass S, Ashrafian H, Neubauer S, Karamitsos TD (2014) Adenosine stress native T1 mapping in severe aortic stenosis: evidence for a role of the intravascular compartment on myocardial T1 values. J Cardiovasc Magn Reson 16:92
42. Liu A, Wijesurendra RS, Ariga R, Mahmod M, Levelt E, Greiser A, Petrou M, Krasopoulos G, Forfar JC, Kharbanda RK, Channon KM, Neubauer S, Piechnik SK, Ferreira VM (2017) Splenic T1-mapping: a novel quantitative method for assessing adenosine stress adequacy for cardiovascular magnetic resonance. J Cardiovasc Magn Reson 19(1):1

43. Gai ND, Sandfort V, Liu S, Lima JA, Bluemke DA (2016) Dose correction for post-contrast T1 mapping of the heart: the MESA study. Int J Cardiovasc Imaging 32(2):271–279
44. Kuijpers D, Prakken NH, Vliegenthart R, van Dijkman PR, van der Harst P, Oudkerk M(2016) Caffeine intake inverts the effect of adenosine on myocardial perfusion during stress as measured by T1 mapping. Int J Cardiovasc Imaging 32(10):1545–1553
45. Doltra A, Amundsen BH, Gebker R, Fleck E, Kelle S (2013) Emerging concepts for myocardial late gadolinium enhancement MRI. Curr Cardiol Rev 9(3):185–190
46. Flett AS, Hayward MP, Ashworth MT, Hansen MS, Taylor AM, Elliott PM, McGregor C, Moon JC (2010) Equilibrium contrast cardiovascular magnetic resonance for the measurement of diffuse myocardial fibrosis: Preliminary validation in humans. Circulation 122(2):138–144
47. Coelho-Filho OR, Shah RV, Mitchell R, Neilan TG, Moreno H Jr, Simonson B, Kwong R, Rosenzweig A, Das S, Jerosch-Herold M (2013) Quantification of cardiomyocyte hypertrophy by cardiac magnetic resonance: implications for early cardiac remodeling. Circulation 128(11):1225–1233
48. Weingartner S, Messner NM, Budjan J, Lossnitzer D, Mattler U, Papavassiliu T, Zollner FG, Schad LR (2016) Myocardial T-1-mapping at 3 T using saturation-recovery: reference values, precision and comparison with MOLLI. J Cardiovasc Magn Reson 18:84
49. Coelho-Filho OR, Mongeon FP, Mitchell R, Moreno H Jr, Nadruz W Jr, Kwong R, Jerosch-Herold M (2013) Role of transcytolemmal water-exchange in magnetic resonance measurements of diffuse myocardial fibrosis in hypertensive heart disease. Circ Cardiovasc Imaging 6(1):134–141
50. Nickander JTR, Jakobsson V, Kellman P, Xue H, Sigfridsson AUM (2017) Quantification of myocardial blood volume reserve by adenosine stress native T1 mapping—validation with adenosine stress ECV mapping. 20th Annual SCMR Scientific Sessions Abstract Supplement. 2017:764
51. Fahreus R (1929) The suspension stability of blood. Physiol Rev 9:241–274
52. Piechnik SK, Chiarelli PA, Jezzard P (2008) Modelling vascular reactivity to investigate the basis of the relationship between cerebral blood volume and flow under CO_2 manipulation. Neuroimage 39(1):107–118
53. Li W, Grgac K, Huang A, Yadav N, Qin Q, van Zijl PC (2016) Quantitative theory for the longitudinal relaxation time of blood water. Magn Reson Med 76(1):270–281
54. Zhang X, Petersen ET, Ghariq E, De Vis JB, Webb AG, Teeuwisse WM, Hendrikse J, van Osch MJ (2013) In vivo blood T(1) measurements at 1.5T, 3T, and 7T. Magn Reson Med 70(4):1082–1086
55. Blatt MA, Suksaranjit P, Wilson B, DiBella EVR (2017) Assessing the repeatability of ECV mapping without hematocrit measurement at 3T. Paper presented at: 20th Annual SCMR Scientific Sessions, Washington, DC
56. Croisille P, De Bourguignon C, Chazot A, Viallon A (2017) Are synthetic haematocrit values derived from blood T1 a good substitute for blood samples to achieve accurate ECV calculation? 20th Annual SCMR Scientific Sessions Abstract Supplement 2017:146
57. Rahman O, Chow K, Barker AJ, Markl M, Carr J, Collins JD (2017) Derivation and validation of synthetic ECV calculation from blood pool T1 values at 3T MRI. Paper presented at: 20th Annual SCMR Scientific Sessions, Washington, DC
58. Raucci JF, Christensen JT, Hernandez LE, Markham LD, Xu M, Slaughter JC, Parra DA, Soslow JH (2017) Synthetic hematocrit derived from the longitudinal relaxation of blood can lead to clinically significant errors in measurement of extracellular volume fraction Paper presented at: 20th Annual SCMR Scientific Sessions, Washington, DC.